The effect of misfit on heterophase interface energies

2002 J. Phys.: Condens. Matter 14 2877

(http://iopscience.iop.org/0953-8984/14/11/307)

INSTITUTE OF PHYSICS PUBLISHING JOURNAL OF PHYSICS: CONDENSED MATTER

J. Phys.: Condens. Matter **14** (2002) 2877–2900 PII: S0953-8984(02)29837-9

The effect of misfit on heterophase interface energies

R Benedek[1], **D N Seidman**[1] **and C Woodward**[2,3]

[1] Department of Materials Science and Engineering, Northwestern University, Evanston, IL 60208, USA
[2] Air Force Research Laboratory, Materials and Manufacturing Directorate, Wright Patterson AFB, OH 45433-7817, USA

Received 18 October 2001, in final form 4 January 2002
Published 8 March 2002
Online at stacks.iop.org/JPhysCM/14/2877

Abstract

Most previous atomistic simulations of heterophase interfaces have neglected *misfit*, the discrepancy between the interatomic length scales parallel to the interface of the two phases. The obstacles to quantitative calculations of interface energies in the presence of misfit are assessed. The most straightforward approach is to perform simulations for a supercell whose size is of the order of the cube of the smallest *common periodic length scale* (essentially the coincidence-site-lattice periodicity), which varies inversely with the misfit parameter. Such supercells typically contain at least thousands of atoms. First-principles simulations are highly accurate, but are feasible only for a few selected heterophase interfaces with large misfit. Classical interatomic potentials, on the other hand, are efficient numerically, but their accuracy has not been demonstrated in the context of heterophase interface calculations. An approximate formulation of the interface energy is presented here which can be evaluated numerically by first-principles calculations for supercells of only moderate size. This formulation explores the relationship between the interface energies for coherent and semi-coherent interfaces. A numerical application to an interface between tetragonal TiAl and perovskite Ti_3AlC is presented.

1. Introduction

Heterophase interfaces are a ubiquitous feature of advanced materials. They appear prominently in a wide variety of intricately engineered components designed for structural, electronic and functional applications. To model accurately the physical properties of such components requires that the interface atomic and electronic structures and energies be described in a realistic manner. Powerful atomic-resolution experimental probes, such as high-resolution electron microscopy [1–3], spatially resolved electron-energy-loss spectroscopy [4], Z-contrast electron microscopy [5, 6], atom-probe field-ion microscopy [7, 8], scanning-tunnelling microscopy [9, 10] and x-ray scattering techniques [11], have advanced our ability to

[3] Materials Research Division, UES Inc., 4401 Dayton-Xenia Rd, Dayton, OH 45432, USA.

characterize the structure and chemistry of heterophase interfaces. Nevertheless, ambiguities in the interpretation of the experimental observations in many instances cannot be resolved readily from experimental considerations alone. Ideally, theory and simulation can help resolve such ambiguities, as well as in making independent predictions.

The simulation of the atomic structures and particularly the energies of real heterophase interfaces, with misfit included, is the subject of this paper. Misfit refers to the non-matching of the atomic spacings (and possibly also bond angles) parallel to the interface of the two phases that comprise the interface. Misfit is of importance because it influences essentially all physical properties of heterophase interfaces, particularly adhesion and mechanical properties. Quantitatively, misfit is often defined as the strain required to make a film coherent with a substrate [2]:

$$\epsilon_m = (a_s - a_f)/a_f \tag{1}$$

where a_s and a_f are substrate and film lattice constants parallel to the interface. For bulk interfaces, a more symmetrical (albeit less physical) definition is sometimes preferred:

$$\epsilon_m = 2(a_1 - a_2)/(a_1 + a_2). \tag{2}$$

A more general definition of misfit that does not assume identical surface-unit-cell shapes of the two phases was recently proposed [12]:

$$\epsilon_m = 1 - (2\Omega)/(S_1 + S_2) \tag{3}$$

where Ω represents the area of overlap of surface unit cells with areas S_1 and S_2. Equation (3) is essentially equivalent to (1) for interfaces for which the latter is applicable. For simplicity, however, equation (1) will be employed in this paper.

We restrict our consideration to clean and atomically sharp interfaces between crystalline phases. Inter-diffusion and reaction layers [13], brazing [14], spinodal decomposition, amorphous [15] and liquid metal/ceramic interfaces [16] and functionally graded materials [17] will not be addressed. Of course, diffuse interfaces are of considerable importance; however, sharp interfaces are in our judgment more amenable to quantitative study at present, both experimentally and theoretically. To model diffuse interfaces and spinodal decomposition, a continuum treatment, particularly the phase-field approach [18, 19], is often appropriate. For the types of interface to be addressed here, which are assumed both structurally and chemically sharp, atomic-scale models represent the most suitable theoretical framework, as we discuss below. Our discussion addresses only interfaces between inorganic materials, for which the interface can be assumed to perturb a highly localized region of microscopic dimensions in the vicinity of the interface. Such an assumption may not be valid in the case of soft matter, with long-chain molecules, which therefore must be treated with different methods [20].

Heterophase interfaces arise in several different morphologies and geometries. Among the most common are film/substrate [2], inclusions embedded in a matrix [21] and multilayers. Continuum elasticity theory can treat these different geometries individually, at least to some extent [22]. In the atomistic treatments that are the main subject of this paper, however, the multilayer geometry, with periodic boundary conditions in three dimensions, is strongly preferred, for computational reasons. A slab geometry also comes under consideration in certain cases. A drawback of the slab geometry is that the properties of the free surfaces of phases 1 and 2 must then be accounted for, an undesirable complication. Except where otherwise noted, we will consider the multilayer geometry, with three-dimensional periodicity and two identical interfaces per unit cell. Our primary focus is on interfaces between bulk phases, and therefore we wish to ascertain limiting values of interface properties for widely spaced layers.

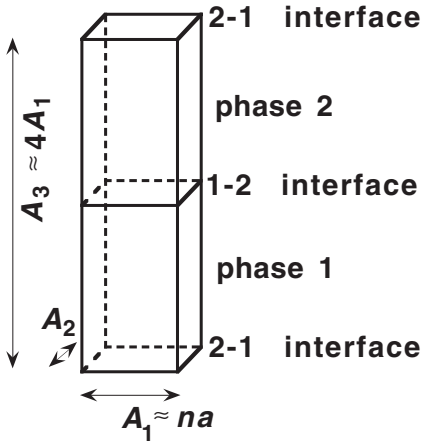

Figure 1. A schematic illustration of the periodic unit cell used for calculation of heterophase interface properties, based on a multilayer geometry. Each unit cell contains two identical interfaces between phases 1 and 2; the interfaces at the top and bottom of the cell are equivalent, by periodicity. The cell dimensions are A_1 and A_2 parallel and A_3 perpendicular to the interface. The parallel dimensions are determined by the misfit dislocation spacing, n. A_3 should be chosen sufficiently large that the regions far from the interfaces (at a point equidistant from two adjacent interfaces, say) are representative of the bulk. The bulk-like regions must be at a distance at least of the order of A_1 (or A_2) from the interface, and thus A_3 should be at least about four times the parallel cell dimension.

Even for a sharp interface with two-dimensional periodicity in the plane of the interface, the number of atoms in the multilayer unit-cell, N, is typically large compared with the number of atoms in the primitive unit cells of the respective crystalline phases on either side of the interface. A rough estimate of the minimum cell size required for the calculation of bulk interface properties is

$$N \sim 4n^3 \tag{4}$$

atoms, where n is the spacing of misfit dislocations[4], which is given essentially by the inverse of the misfit [2]:

$$na_{\mathrm{row}} = b_\perp/\epsilon_m. \tag{5}$$

Here, $b_\perp$ is the component of the Burgers vector parallel to the interface and perpendicular to the misfit dislocation line, and a_{row} is the spacing of atomic rows in the interface perpendicular to the misfit dislocation line. In further discussions, we assume for simplicity that $b_\perp = a_{\mathrm{row}}$, although this is violated for dissociated misfit dislocations. Equation (4) assumes monatomic Bravais lattices for both phases, and therefore represents a lower bound for the number of atoms in the cell.

The strain field of the misfit dislocation network is assumed to penetrate into each phase by a distance of the order of the dislocation spacing. The size of the computational cell perpendicular to the interface is thus also taken to be proportional to n. The factor of 4 in equation (4) includes a factor of 2 for the two interfaces per wavelength of the multilayer, and a factor of 2 for the two phases on opposite sides of each interface, see figure 1 for a schematic illustration of the unit cell.

[4] This relation should not be considered quantitative since it neglects possible complications such as different numbers of atoms in the surface unit cells of the two phases, and the existence of more that one independent misfit parameter for a given interface.

A complication associated with the multilayer geometry depicted in figure 1 is that for the bulk stacking of atomic layers in phases 1 and 2, there is no guarantee that the two interfaces in the unit cell of figure 1 are identical. An ambiguity occurs, for example, when the layers have hexagonal geometries, and ABC stacking sequences apply. Identical interfaces can be achieved by the introduction of a twin boundary in each phase. In most cases, the twin boundaries have interface energies that are considerably lower, and represent much smaller perturbations, than the heterophase interfaces. Furthermore, the properties of the twin boundaries may be readily calculated separately, and subtracted to determine the properties of the heterophase interfaces.

For most heterophase interfaces of interest, the periodicity parameter n is greater than about 10. Thus, a typical unit cell suitable for the simulation of a heterophase interface with misfit contains not less than several thousand atoms. A cell size of several thousand atoms is relatively modest by the standards of modern molecular dynamics or Monte Carlo simulations, but large by the standards of first-principles [23], or even semi-empirical [24], electronic structure computation. Considerably larger cell sizes, with n greater than 20, occur in many systems of interest [25].

The large cell size is often a significant obstacle to realistic simulations, but other technical obstacles are perhaps even more troublesome. First, we note that the chemical bonding in the vicinity of the interface may have a mixed and poorly defined character. An oxide–metal interface, for example, may comprise aspects of metallic, covalent, dispersion and ionic bonding simultaneously. Since the interface is the focus of attention, it is clearly desirable to treat the interactions at the interface with an accuracy comparable to that with which the bulk phases on either side of the interface are treated. Another critical feature is that misfit induces an interface structure that is not precisely coherent. To ascertain the detailed interface structure is a challenging problem, because, for one thing, the relaxation pattern that the system adopts is not uniquely determined by symmetry considerations, although symmetry plays an important role. For example, dissociation of the misfit dislocation network into partial dislocations [26] is often possible, but may occur only fractionally. In such cases, the extent of dissociation is determined by the interatomic interactions in the vicinity of the interface. Furthermore, the compositions and densities of the interface layers may differ from those of bulk layers of the two phases [25].

Interface misfits vary widely, depending on the particular interface and crystallographic orientation under consideration. Large misfits can in some instances be greatly reduced simply by a rotation of one of the phases relative to the other [27]. The smallest observed spacing of misfit dislocations is about $n = 5$. One such system with small periodicity in the interface plane is MnO/Cu [28]. Values of n below about 10 correspond to very large misfit. At the other extreme, minute misfits (with n as large as 10^3 or more) can be engineered, for example in heterophase interfaces between semiconductor alloys [26]. It is not precisely clear what misfit values can be considered small from a physical point of view. For example, calculation of the interface energy within the coherent-interface approximation is presumably accurate when the misfit is sufficiently small. A theory that 'corrects' the coherent-interface result for the effect of misfit would provide guidance in this regard. An attempt to formulate such a theory is presented in this paper.

The problem of modelling the effect of misfit on interface structure has a long history. The earliest work [29–31] employed continuum elasticity theory. More elaborate continuum formulations have been developed in recent years [32–35]. For the case of layered growth of a film on a substrate (Frank–van der Merwe growth), strained layers occur for sufficiently small film thicknesses, but a network of misfit dislocations becomes energetically favourable when a critical thickness is exceeded [31]. (Other instabilities, such as those associated with the surface of the film, do not concern us here.) This phenomenology provides useful qualitative

insights, and can yield semi-quantitative and even quantitative predictions in some instances. It is, nevertheless, limited in various respects. Although the interaction across the interface must play a key role in determining interface properties, this interaction cannot be directly incorporated into continuum models. The continuum elasticity theory of heterophase interfaces is parametrized in terms of interface elastic moduli, which may be regarded as undetermined effective-medium parameters. Furthermore, in the case of interfaces with large misfit, where the misfit dislocation cores nearly overlap, the applicability of continuum treatments becomes suspect. Also, large atomic displacements from ideal lattice sites, as well as deviations from stoichiometry [36] and bulk layer densities, are outside the scope of continuum formulations.

These considerations, as well as the desire to compare simulation directly with atomic-resolution experimental probes, provide strong motivation for the development of atomistic treatments of heterophase interfaces, which is the theme of this paper. Atomistic simulations of homophase boundaries, namely grain boundaries, have achieved a high level of sophistication and precision [37], but this is not matched by simulations of heterophase interfaces. The lack of suitable interaction models, as mentioned above, has been an impediment. A few examples will suffice to illustrate the state of the art. Interfaces between different metals have been simulated using embedded-atom-method (EAM) potentials [38]. Examples are simulations of Pd–Cu [39], Cu–Ag [40], Ag–Ni and Au–Ni [36, 41] and Al_3Sc–Al interfaces [42]. Metal–nonmetal interfaces have been simulated [43] with the EAM and modified EAM (MEAM) [44]. Heterophase metal–metal interfaces have also been treated with the effective-medium theory [45–47] and the tight-binding second-moment approximation [48], both of which are similar in spirit to the EAM. For metal–metal interfaces, interatomic-potential models such as the EAM may be expected to describe the interface regions with an accuracy somewhat comparable to that for the respective bulk systems. Similar remarks may apply to the treatment of heterophase interfaces between ionic materials [49], in which the interatomic potentials are parametrized within the Born model. The MEAM has recently been applied to oxide–oxide interfaces [50]. Semiconductor heterophase interfaces, for example between different III–V compounds such as InAs/GaAs [51] are of great interest for device applications. Accurate interatomic potentials even for the bulk phases of polar semiconductors are not readily available, however, although recent developments are encouraging [52, 53]. First-principles methods offer an alternative approach, which avoids the arbitrariness of classical interatomic potentials. The inclusion of misfit, however, typically entails unit cells for which the numerical effort is prohibitive. Such an approach was employed for the (110) InAs/GaAs interface [54], but was only possible with the use of a minimal basis set.

Interfaces between materials with different types of bonding, for example, metal–oxide, metal–semiconductor (Schottky barrier) and semiconductor–oxide interfaces, pose even greater difficulties for modelling with classical potentials. Metal–oxide and other ceramic–metal interfaces have received considerable attention. One approach that has been developed in some detail for metal–oxide interfaces is based on image-charge-interaction potentials [55,56].

A huge literature exists on first-principles calculations for ceramic–metal interfaces, including oxide–metal interfaces [12, 57–65] as well as semiconductor–metal interfaces [66, 67], and carbide–metal [68, 69], semiconductor–semiconductor [70], semiconductor–ceramic [71] and ceramic–ceramic [72] interfaces. In addition to the work on bulk interfaces, many studies of adsorbed layers have been performed [73]. The cited references are only representative, and far from comprehensive.

Almost all of the cited first-principles studies were restricted to coherent interfaces, and neglected misfit. In previous work by some of the present authors, interface misfit in oxide–metal interfaces was addressed by following either of two strategies. First, calculations for the interface {222} MgO/Cu have been performed with first-principles methods [74].

MgO/Cu has a repeat distance $n = 6$, for which the calculations are feasible, although highly time-consuming. The second approach is the parametrization of a classical interatomic potential for the interface of interest. A MEAM potential for the Nb/alumina interface has recently been developed [75].

There is a trade-off between the computational efficiency of treatments based on classical interatomic potentials and the physical accuracy of first-principles methods, particularly local density functional theory [23]. The efficiency of classical-potential methods gives them great flexibility. With classical-potential methods, for example, almost arbitrary misfit values can be addressed, dynamical simulations can be performed and mechanical property (such as fracture) simulations are feasible, at least to some extent. Dynamical simulations are of particular interest because heterophase interfaces are typically formed at elevated temperatures. The ability of classical potentials to accurately represent real interfaces, however, has not been demonstrated. There are at the present time few, if any, interatomic potentials for heterophase interface systems with accuracy comparable to first-principles methods. This is particularly true when the phases have dissimilar chemical bonding. Considerable scope exists for further work in this direction, however. The ability of environmentally sensitive potentials (examples are the MEAM [43], variable-charge potentials [76] and bond-order potentials [53, 77]) to interpolate between widely disparate bonding configurations provides a strong incentive for further development. Most existing environmentally sensitive potentials have been derived for monatomic or binary systems, and ternary [75] and higher systems pose an even more severe challenge. The tedious development and validation process that is necessary before the potentials can be employed in production simulations has probably discouraged such efforts, in spite of their promise.

We have noted above that, on the one hand, the treatment of misfitting interfaces directly within local density functional theory is in most cases computationally prohibitive and, on the other, the systematic derivation of accurate environmentally dependent classical potentials for multicomponent systems is as yet an unsolved problem. In the remainder of this paper, we explore a third approach, which exploits the accuracy of first-principles methods, while not requiring the large cell sizes that a direct treatment of the full two-dimensional interface superlattice would entail. The formulation expresses the interface energy for a system with arbitrary misfit in terms of the corresponding energy for the appropriate coherent interface, corrected for strain, misfit dislocations and stoichiometry.

2. Interface energy

A fundamental property of interfaces is their *excess* energy (or free energy), γ, per unit area. Calculation of the interface energy, for example, enables one to determine the relative stability of different interface terminations, when the termination is not unique. Only the termination with the lowest interface energy occurs in thermodynamic equilibrium.

2.1. Coherent interface

We outline in this section the formulation of γ for a coherent heterophase interface. A previous treatment of the surface free energy [78], formulated in terms of the chemical potentials of the different atomic species, can be adapted directly to interfaces [72]. This approach enables the treatment of layers of arbitrary stoichiometry, and is therefore not restricted to orientations in which individual atomic layers parallel to the interface have the same stoichiometry as the respective bulk phases. It was recently applied to a widely studied model oxide–metal interface, Nb {111}–alumina {0001} [59,60]. Both the oxygen and the aluminium terminations

of alumina were considered as functions of oxygen partial pressure (or chemical potential). This interface has a relatively small misfit ($\epsilon = 0.02$) and is plausibly treated as coherent, to a first approximation.

The interface energy is defined as the energy difference between an atomic configuration that includes the interface, and one in which an equivalent number of atoms experience bulk environments. In the case of a periodic multilayer geometry, at low temperatures, it may be expressed in the form

$$\gamma_{\mathrm{p}} = (E(A, n, \epsilon) - N\mu)/2S \tag{6}$$

where an abbreviated notation is adopted for convenience. The energy E is the total free energy per periodic unit cell (cf figure 1) of the multilayer system, which has two identical interfaces with area S (hence the factor of 2 in the denominator of equation (6)). The atomic and cell coordinates of the supercell, for which the energy, E, is evaluated, are assumed to be fully relaxed. The details of the relaxation procedure, however, are not discussed here.

The term $N\mu$ denotes the sum of the chemical potentials of all of the atomic species within the unit cell. Application of the Gibbs phase rule to interfaces with more than two components reveals that not all of the chemical potentials are uniquely determined, and at least one of them may therefore be chosen arbitrarily from within a physically relevant interval [59, 60, 72, 79]. In our treatment, the appropriate chemical potentials are determined for the bulk phases, separately from the calculation of E. An example will be given in section 3. We note that an alternative approach would be to constrain the chemical potentials of phase-2 components to preclude strain-related contributions to γ that scale with the volume (cf equation (8), below). Such a procedure is reasonable if misfit is to be neglected, but would not be harmonious with the formulation of misfit-related energies to be described in succeeding sections.

The array A, the first argument of E in equation (4), contains the basis vectors for the superlattice. The second argument, n, denotes an array of integers that specify the unit-cell periodicity in the plane of the interface, as well as the number of layers of each phase perpendicular to the interface. We will take the first two basis vectors A_1 and A_2 to lie in the plane of the interface, and $A_3 \equiv A_\perp$ refers to the cell dimension perpendicular to the interface. Typically, the basis vectors in the plane of the interface are integer multiples of primitive lattice vectors. For a simple coherent interface, the components of n that define the periodicity in the plane of the interface reduce to unity, and the number of layers of each phase perpendicular to the interface, $n_3(1)$ and $n_3(2)$, are chosen to be relatively small numbers. With a judicious choice of $n_3(1)$ and $n_3(2)$, a multilayer unit cell with at least monoclinic, and in many cases orthorhombic or hexagonal, symmetry may be obtained. The third argument of E, namely ϵ, represents the strain imposed on either or both phases by the selected values of A and n. Although not all three of these arguments are mutually independent, we retain all of them for clarity. For the idealized coherent interface without mismatch, all of the strains vanish. As mentioned above, we adopt the convention that phase 1 is unstrained, and a strain ϵ_m is imposed on phase 2 to achieve coherence in the presence of mismatch.

2.1.1. Thermodynamic limit. Consistency with equilibrium thermodynamics requires that the general definition of the interface energy between two bulk phases, γ_∞, refer to unconstrained semi-infinite phases in contact, rather than to supercells, constrained by periodicity. The formulation of γ_{p}, adopted for computational convenience, must therefore be regarded only as an approximation to γ_∞, although one expects that it will often be an excellent one in practice. It is reasonable to suppose that equation (6) becomes increasingly accurate and that γ_{p} approaches γ_∞ in the limit of large cell dimensions, A. Owing to the incommensurate length scales (lattice constants) of the two phases, however, the precise meaning of the limit of large cell dimensions is ambiguous, mathematically.

If we set aside the formal difficulties associated with an incommensurate interface, and consider instead the idealized problem of a coherent interface without mismatch, the correspondence between γ_∞ and γ_p becomes clear. With the assumption of coherence, only the limit for scaling in the perpendicular direction, with respect to the variables A_3 (the cell vector perpendicular to the interface), $n_3(1)$ and $n_3(2)$ (both of which are proportional to A_3) is required. Rapid convergence with respect to these variables is guaranteed by the exponential decay with distance of the perturbation to electronic properties induced by the interface [80], and the lattice relaxation induced by the interface [81]. Thus, the convergence of γ_p to a limiting value as the perpendicular dimension increases is expected to be rapid, in the case of vanishing mismatch. Similar arguments apply when the mismatch is finite, but commensurate. Incidentally, in the context of elasticity theory, the relatively short range of the perturbation introduced by a surface or an interface is referred to as St Venant's principle [82].

2.1.2. Misfit strain energy. Let us consider the case of a non-zero misfit:

$$\epsilon_m = [a_\parallel(1) - a_\parallel(2)]/a_\parallel(2) \tag{7}$$

where the lattice constants in the plane of the interface, $a_\parallel(1)$ of phase 1 and $a_\parallel(2)$ of phase 2, differ (for lower-symmetry interfaces, in which at least one of the phases has two independent lattice constants in the plane of the interface, two different misfit parameters occur). We consider the coherent interface that is created by application of the appropriate strain to phase 2. For this coherent interface, the strain parameter $\epsilon(2) = \epsilon_m$. The energy associated with this strain contributes

$$\Delta\gamma_p \sim C(2)\epsilon(2)^2 A_\perp \tag{8}$$

to γ_p, as defined by equation (6), where $C(2)$ is an appropriate elastic modulus for phase 2, which can be expressed in terms of the elastic moduli of the bulk phase [83]. This contribution to γ_p is proportional to the perpendicular dimension of the multilayer unit cell, $A_\perp$. The quantity γ_p therefore does not approach a limiting value for large $A_\perp$, and contains a volume-dependent strain term in addition to the contribution from the interface region. It is therefore not strictly a superficial (area-proportional) property. The presence of this term implies, of course, that a coherent interface is energetically unfavourable, except for sufficiently thin layers.

2.2. Semi-coherent interface: interface superlattice

Consider an interface between materials with commensurate lattice spacings, i.e.,

$$\epsilon_m = 1/n \tag{9}$$

where n is an integer. Under these circumstances, the (bulk) strain, and hence the strain energy contribution to γ, equation (8), can be suppressed by constructing a supercell with appropriate dimensions. The cell dimensions parallel to the interface are selected to coincide with the smallest length scale for which both bulk phases are periodic:

$$A_\parallel = na_\parallel(1) = (n \pm 1)a_\parallel(2). \tag{10}$$

For each n phase-1 unit cells along an atomic row in the plane of the interface, there are $n \pm 1$ phase-2 unit cells in the layer on the opposite side of the interface. $A_\parallel$ is the *smallest common periodic length scale* and is therefore directly related to the coincidence-site-lattice spacing [87]. The plus or minus is determined by whether the lattice constant for phase 1 or that for phase 2 is larger. The unit cell of such a superlattice is approximately n^2 times as large as that for the coherent interface (per atomic layer parallel to the interface).

In general, of course, the mismatch for real heterophase interfaces is incommensurate and

$$\epsilon_m = (n \pm \delta)^{-1} \tag{11}$$

where $0 < \delta < 1/2$. The quantity δ is proportional to the misfit strain of the superlattice specified by equation (10). For non-zero δ, the strain in phase 2 is considerably reduced, compared to that of the coherent interface:

$$\epsilon_{\text{super}} \sim \delta/n^2 \ll \epsilon_m. \tag{12}$$

Accordingly, the periodic superlattice becomes unstable when the perpendicular cell dimension A_3 (or, more precisely, the number of layers $n_3(2)$ of phase 2) exceeds a critical value. (This instability is analogous to the instability of the coherent interface that occurs at a much smaller value of $n_3(2)$.) It is reasonable to speculate that when the perpendicular cell dimension exceeds this critical value, the ground-state interface structure becomes *quasiperiodic*. Nevertheless, in practice, a periodic superlattice may often represent an excellent approximation to the true ground-state structure, even when the latter is not strictly periodic. Thus, electron microscopy observation of a wide variety of interfaces indicates that interfaces with misfit often exhibit essentially periodic arrays of misfit dislocations [84]. In what follows, we proceed on the assumption that a two-dimensionally periodic system with periodicity specified by equation (10) is an excellent approximation to the true ground-state interface structure.

2.3. Relationship between the semi-coherent and coherent interface

In the remainder of this paper, we develop a formulation in which the interface energy for a semi-coherent interface is expressed as the sum of the corresponding coherent-interface energy, γ_{coh}, calculated with equation (6), and a correction term:

$$\gamma_{\text{semi}} = \gamma_{\text{coh}} + \Delta\gamma. \tag{13}$$

The explicit form of the correction term $\Delta\gamma$ for a lattice model will now be explored. Apart from the utility of this scheme for calculating properties of particular interfaces, such a formulation may eventually yield insights into the issues of misfit dislocation stand-off [36, 85], and the competition between interface semi-coherency and incoherency [86], although these subjects are not addressed specifically in this paper. It may also enable us to quantify whether particular values of the misfit ϵ_m should be regarded as either 'large' or 'small'. Only by drastically reducing the number of degrees of freedom can such issues be addressed systematically.

The usefulness of equation (13) as a practical computational scheme, of course, depends on whether approximations for $\Delta\gamma$ that are both tractable and accurate are available. We will seek approximations in which the calculations of $\Delta\gamma$ involve cell sizes that are of the same order as those used for the calculation of γ_{coh}, and are at any rate much smaller than the cell size given by equation (4). The smaller cell sizes will be readily accessible to first-principles methods, unlike the supercells discussed in the previous section. The approximations proposed below for $\Delta\gamma$ are to some extent uncontrolled, and their validity must be tested thoroughly before their efficacy can be judged. The presentation in this section, however, will be limited to an exposition of the main ideas. In the following section a numerical application will be presented, as well as a discussion of possible tests of the validity of the approximations.

Continuum elasticity theory formulations of the interface energy of a thin film on a substrate yield insight into the form of $\Delta\gamma$. Tersoff and Tromp [89] write the film–substrate interface energy associated with misfit dislocations in a film of thickness t as

$$\gamma_{\text{film}} = 2\lambda\kappa + C(\epsilon_m - b_\perp\kappa)^2 t \tag{14}$$

where λ is the energy per unit length of a misfit dislocation, κ is the misfit dislocation density (zero for a strained layer and $1/n$ for a periodic network) and $b_\perp$ is the projection of the Burgers vector on the plane of the interface, and perpendicular to the misfit dislocation line (cf equation (5)). The first term in this phenomenological expression represents the energy of the misfit dislocation network, whereas the second term represents the strain energy, and is analogous to equation (8). One of the primary motivations for developing a lattice theory is the lack of a systematic procedure to evaluate the parameters in this expression, such as λ.

In attempting to formulate a lattice model, it is helpful to postulate an explicit sequence of transformations that takes the coherent interface into a semi-coherent one. We consider the transformation to occur in three separate steps, which are illustrated in figure 2. The starting configuration is a coherent interface, in which the interface cell has been relaxed to its minimum-energy configuration with respect to the atomic-layer coordinates perpendicular to the interface, as well as the translation state parallel to the interface. This relaxation would be performed, for example, in the evaluation of the coherent-interface energy using equation (6). The resultant atomic arrangement of the interface layers is illustrated schematically in figure 2(a). In this figure the atomic coordinates of the layers of phase-1 atoms (denoted by crosses) and phase-2 atoms (denoted by filled circles) adjacent to the interface, projected onto the plane of the interface, are plotted. In the hypothetical interface system illustrated in this figure, the phases have square-lattice layers with an assumed lattice constant ratio $a_1/a_2 = 5/4$, and a resultant misfit

$$\epsilon_m = 0.25. \tag{15}$$

For the coherent interface, the primitive interface unit cell contains only a single atom per layer, and the parallel cell dimension $A_\parallel = a(1)$. Four unit cells are bounded by solid lines in figure 2(a). It is assumed that the equilibrium translation state corresponds to the on-top configuration.

In the first step of the transformation (figure 2(b)), columnar 4×4 blocks of phase-2 atoms are contracted to their assumed bulk lattice constant, $a(2) = 0.8a(1)$, while phase-1 atomic positions are held fixed. Solid lines are drawn in the middle of the resultant gaps between the blocks. The four unit cells bounded by these lines have the dimensions of the smallest common periodic length scale, $A_\parallel = 4a(1) = 5a(2)$, which corresponds to equation (10).

The gaps between the phase-2 blocks occur because the interface stoichiometry is changed. To correct for this difference in stoichiometry, additional phase-2 atoms are considered transferred from a reservoir to 'unoccupied' phase-2 lattice sites within the gaps. These transferred atoms are represented by open circles in figure 2(c). We refer to the atomic configuration in this panel as the *reference incoherent state*. The interface-plane-projected positions of phase-1 atoms correspond to perfect-lattice sites for bulk phase 1 and similarly for phase 2. Accordingly, figure 2(c) represents a conceptual intermediate state and not a 'real' incoherent interface.

The final step in the transformation is to allow the interface in figure 2(c) to relax to equilibrium, under the influence of both interphase and intraphase interactions, and the resultant configuration is illustrated schematically in figure 2(d). The atoms within the interior of the cells (i.e., distant from the solid lines) relax toward the on-top position to minimize the interphase interactions, but cannot achieve precise registry because the intraphase interactions resist distortion of bond lengths and angles from their ideal bulk values. The atoms that lie on the solid lines represent misfit edge dislocations. The configuration in figure 2(d) is referred to as semi-coherent.

The interface energy difference between the atomic configuration depicted in figure 2(d) and that in figure 2(a) is $\Delta\gamma$. The intermediate steps, figures 2(b) and (c), are arbitrary,

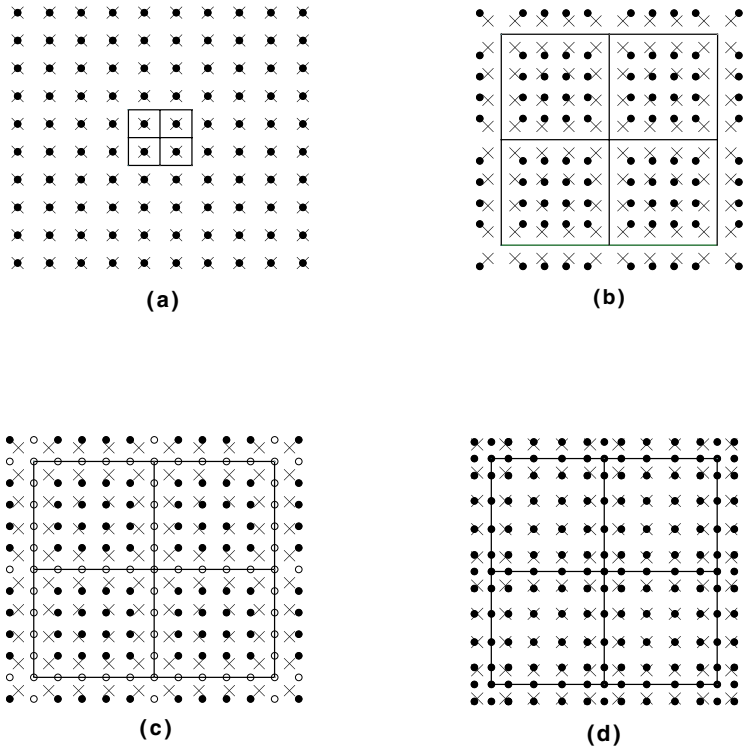

Figure 2. A schematic illustration of the transformation of a coherent interface to a semi-coherent interface. A hypothetical interface between crystals with square-lattice atomic layers normal to the interface is shown. The crosses represent phase-1 atoms and the filled circles phase-2 atoms in the atomic layers adjacent to the interface, projected onto the plane of the interface. The phase-2 layer in panel (*a*) is strained in tension to achieve coherency with phase 1. A misfit $\epsilon_m = 0.25$ is assumed. In panel (*b*), blocks of phase-2 atoms are contracted to the bulk lattice constant of phase 2. In panel (*c*), phase-2 atoms from a reservoir are transferred to the sites indicated by open circles to compensate for the change in stoichiometry that occurs when the coherency strain is removed. The configuration in panel (*c*), in which no in-layer relaxation has occurred, is referred to as the reference incoherent state. The semi-coherent interface, panel (*d*), refers to the configuration in which atoms are allowed to relax to equilibrium. See the text for further discussion.

and the formulation of $\Delta\gamma$ must be independent of them, in principle. Nevertheless, we find the reference incoherent interface, figure 2(*c*), useful in the approximation scheme discussed below.

To proceed, we adopt the assumption that contributions to the interface energy can be attributed, approximately, either to interphase or intraphase interactions:

$$\Delta\gamma = \Delta\gamma_{\text{intra}} + \Delta\gamma_{\text{inter}} \tag{16}$$

where the terms on the right-hand side refer to intraphase (within each of the phases) and interphase (across the interface) contributions. In a classical-potential treatment based on pairwise interatomic interactions, for example, such a separation is evident, but in treatments in which energies are calculated either with environmentally dependent classical interatomic potentials or with first-principles techniques, no such decomposition can be made in a rigorous way. Only with such an approximation, however, can further progress be made.

The intraphase interactions are expressed as

$$\Delta\gamma_{\text{intra}} = \Delta\gamma_{\text{intra}}^{\text{strain}} + \Delta\gamma_{\text{intra}}^{\text{rel}} \tag{17}$$

where the first term on the right-hand side gives the contributions associated with the transformation from figures 2(*a*) to (*c*), and the second term refers to the to the transformation from figures 2(*c*) to (*d*). To evaluate the strain term, we calculate the energy difference between unstrained (figure 2(*c*)) and strained (figure 2(*a*)) slabs of phase 2. To this must be added a chemical-potential contribution that corrects for the change in interface stoichiometry between figures 2(*a*) (or (*b*)) and (*c*). On the basis of these considerations, we write

$$\Delta\gamma_{\text{intra}}^{\text{strain}} = E(A_{\text{bulk}}, 1, 0; 2)/2S_{\text{bulk}} - E(A_{\text{coh}}, 1, \epsilon_m; 2)/2S_{\text{coh}} + \Delta(N\mu/2S). \tag{18}$$

The unstrained parallel cell dimension A_{bulk} is the bulk lattice constant $a(2)$ and A_{coh} is the cell dimension used in the calculation of γ_{coh}, namely $a(1)$. S_{bulk} is the cell area corresponding to the bulk lattice constant $a(2)$ and S_{coh} is the cell area employed in the coherent-interface calculation.

The layer atomic density, parallel to the interface, of phase-2 atoms in the semi-coherent (or incoherent) interface differs from that in the coherent interface by the factor $(1 + \epsilon_m)^2$. Therefore, a fraction

$$d = (1 + \epsilon_m)^2 - 1 \tag{19}$$

of phase-2 atoms ($d = 9/16$ for the model interface in figure 2, but is considerably smaller for most realistic interfaces) is transferred from a thermodynamic reservoir to sites in each phase-2 layer. The sites denoted by open circles in figure 2(*c*) are considered to be filled by this process. Using equation (19), we can write the final term in equation (18) as

$$\Delta(N\mu/2S) = -dN_2\mu_2/2S_{\text{coh}}. \tag{20}$$

The density of phase-1 atoms is assumed unchanged in figure 2(*d*) relative to (*a*), and hence there is no contribution to $\Delta\gamma$ associated with $N_1\mu_1$.

Before we address the intraphase relaxation term, $\Delta\gamma_{\text{intra}}^{\text{rel}}$, we consider the interphase contributions, $\Delta\gamma_{\text{inter}}$. Contributing to the latter term are both (i) the reduction in interface adhesion per phase-2 interface atom and (ii) the change in stoichiometry by the factor $(1 + d)$. We approximate the difference in adhesion in terms of results for coherent interfaces with different *parallel translation states* (cf figure 3).

It is reasonable to identify the (interphase) bonding across a coherent interface with the (modified) adhesive or separation energy:

$$W = [E(A_{\text{coh}}, 1, \epsilon_m; 1) + E(A_{\text{coh}}, 1, \epsilon_m; 2) - E(A_{\text{coh}}, 1, \epsilon_m; 12)]/2S_{\text{coh}} \tag{21}$$

where $E(A_{\text{coh}}, 1, \epsilon_m; 12)$ is calculated for the multilayer unit cell with two interfaces (figure 1). $E(A_{\text{coh}}, 1, \epsilon_m; 1)$ and $E(A_{\text{coh}}, 1, \epsilon_m; 2)$ refer to the energies of phase-1 and phase-2 slabs, respectively, with the atomic configurations in the slabs constrained to be identical to those in the relaxed coherent-interface cell, so that W represents, as closely as possible, a purely interphase energy. In this respect, the present treatment of adhesive (or separation) energy differs from the standard one, in which the slabs are relaxed separately [88]. In further discussions, we adopt the convention that the symbol W is always normalized to S_{coh}, even in our treatment of semi-coherent interfaces, in which phase 2 has a different atomic density; the atomic density will be accounted for by the factor D.

To evaluate equation (21) the parallel translation state must be specified. For the model interface between square-lattice atomic layers schematically illustrated in figure 2, there are three symmetric parallel translation states, which are depicted in figure 3. The three panels correspond to the on-top site (also shown in figure 2(*a*)), the bridge site and the hollow site. (On-top, bridge and hollow sites also occur for interfaces between layers with Bravais lattices of other types, such as triangular lattices.) We represent the translation state by a vector h_j parallel to the plane of the interface, where $j = 1$ corresponds to the preferred translation,

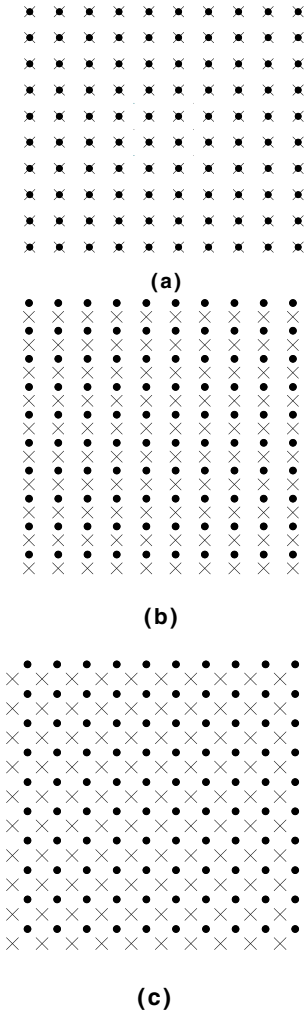

Figure 3. An illustration of the three symmetric translation states for the square-lattice interface (cf figure 2). The panels (*a*), (*b*) and (*c*) correspond to the on-top, bridge and hollow configurations respectively.

the on-top configuration in our illustrative example, figure 2. The equilibrium adhesive energy for a coherent interface is then

$$W = W_{h_1} \tag{22}$$

where $E = E_{h_1}(A_{\mathrm{coh}}, 1, \epsilon_m; 12)$ is evaluated for the energetically preferred translation state.

Atoms that lie within the interface layers of semi-coherent interfaces experience a variety of coordination environments. Thus, some atoms are situated in hollow-site, bridge-site and on-top configurations, while others are 'off-centre' and thus not precisely in high-symmetry locations. In figure 2(*d*), we see that atoms far from the cell boundaries experience on-top environments, similar to the coherent interface shown in figure 3(*a*) (or 2(*a*)). The misfit dislocation core atoms along cell boundaries experience approximate bridge-site environments similar to those in the coherent interface illustrated in figure 3(*b*), and cell-corner atoms experience hollow-site environments similar to those in the coherent interface illustrated in figure 3(*c*).

These considerations motivate the approximation of the interphase contribution to the interface energy difference, $\Delta\gamma_{\text{inter}}$, as

$$\Delta\gamma_{\text{inter}} = W_{h_1} - \langle W(\text{semi})\rangle \tag{23}$$

where the procedure for evaluating the average $\langle W(\text{semi})\rangle$ is considered in the following subsection. By combining the results of equations (16), (17) and (23), we have

$$\Delta\gamma = \Delta\gamma_{\text{intra}}^{\text{strain}} + \Delta\gamma_{\text{intra}}^{\text{rel}} + W_{h_1} - \langle W(\text{semi})\rangle. \tag{24}$$

Relations for $\Delta\gamma_{\text{intra}}^{\text{strain}}$ and W_{h_1} have been given in equations (18) and (21), respectively. Approximations for $\Delta\gamma_{\text{intra}}^{\text{rel}}$ and $\langle W(\text{semi})\rangle$ are developed below.

2.3.1. Evaluation of $\langle W\rangle$. We consider the average adhesive energy $\langle W(\text{semi})\rangle$; an analogous relation will also apply to the average in the reference incoherent state, $\langle W(\text{incoh})\rangle$. We assert that these averages can be approximated reasonably as appropriate averages of W_{h_j}. Thus, off-centre phase-2 interface atoms, which do not lie precisely in on-top, bridge or hollow sites, are assigned to the symmetry types that they most closely resemble. Accordingly, we write

$$\langle W\rangle = D\sum f_j W_{h_j} \tag{25}$$

where f_j represents the fraction of phase-2 interface atoms assigned to type j; the sum of f_j is normalized to unity. The factor D, the relative density, is given by $1 + d$—since W_{h_j} is calculated for the coherent interface (figure 2(*a*)) and is normalized to the cell area S_{coh} of the coherent interface. D accounts for the change in density of a layer of phase 2 at the semi-coherent interface relative to the coherent interface.

In the case of square- or triangular-lattice interfaces, the difference

$$W_{h_1} - \sum f_j W_{h_j} = -(f_2\,\Delta W_{h_2} + f_3\,\Delta W_{h_3}) \tag{26}$$

where $\Delta W_{h_j} = W_{h_j} - W_{h_1}$. The adhesive energies obtained by evaluating $E = E_{h_j}(A_{\text{coh}}, 1, \epsilon_m; 12)$ for $j = 2, 3$ with interlayer and interface separations identical to those corresponding to the equilibrium translation state h_1 will be referred to as $W_{h_j}(\text{incoh})$. The weights $f_j(\text{incoh})$ for the incoherent interface are for simplicity taken to be proportional to relative multiplicity of the symmetry sites of type j. For illustration, let us assume that they are equal, i.e., $f_j(\text{incoh}) = 1/j_{\max}$. For $j_{\max} = 3$, we then have

$$\langle W\rangle - W_{h_1} = (\Delta W_{h_2} + \Delta W_{h_3})/3 + d(W_{h_2} + W_{h_3}) \tag{27}$$

where W refers to the reference incoherent state.

As mentioned above, the reference incoherent interface (figure 2(*c*)) is unstable, because non-zero atomic forces exist, both parallel and perpendicular to the interface. The semi-coherent interface refers to the atomic configuration after relaxation to equilibrium. Simulations of the relaxed atomic structure of a semi-coherent MgO/Cu interface were presented recently [74]. The relaxed interface structure shows an increased number of atoms in coherent-like patches, relative to the reference incoherent state: $f_1(\text{semi}) > f_1(\text{incoh})$; the opposite inequality holds for subscripts $j = 2, 3$. This feature has been portrayed schematically in figure 2(*d*), where phase-2 atoms (filled circles), except those located on misfit dislocation lines, have been displaced towards neighbouring on-top sites, relative to their counterparts in figure 2(*c*). Assigning subscript 2 to atoms lying on dislocation lines and 3 to those located at line intersections, we make the following approximations:

$$f_2(\text{semi}) \approx 2/n \approx 2\epsilon \tag{28}$$

and

$$f_3(\text{semi}) \approx 2/n^2 \approx 2\epsilon^2. \tag{29}$$

These relations are based on the assumption that all atoms not located on dislocation lines lie in semi-coherent patches with local environments that correspond to the strongly bonding $j = 1$ symmetry. This assumption is, of course, somewhat idealized.

The preceding discussion is related to the atomic relaxation parallel to the interface that accompanies the transformation from the reference incoherent interface to the semi-coherent interface. This parallel relaxation redistributes the fractions f_j. In addition to the parallel relaxation, the atomic coordinates perpendicular to the interface also relax and yield an additional energy gain:

$$\Delta W(\text{perp}) = \sum f_j(\text{semi})[W_{h_j}(\text{semi}) - W_{h_j}(\text{incoh})] \tag{30}$$

where $W_{h_j}(\text{semi})$ represents the adhesive energy obtained with the layer spacings allowed to relax in the calculation of $E = E_{h_j}(A_{\text{coh}}, 1, \epsilon_m; 12)$ for $j = 2, 3$.

If we write the adhesive energy for the semi-coherent interface as

$$\langle W(\text{semi})\rangle = D \sum f_j W_{h_j}(\text{semi}) \tag{31}$$

then the total gain in interphase energy in the semi-coherent interface, relative to the incoherent interface, including both parallel and perpendicular relaxation, can be expressed as

$$\langle W(\text{incoh})\rangle - \langle W(\text{semi})\rangle \approx (1/3 - 2\epsilon)\,\Delta W_{h_2} + (1/3 - 2\epsilon^2)\,\Delta W_{h_3} + \Delta W(\text{perp}). \tag{32}$$

2.3.2. Intraphase interaction contributions to relaxation energy. A gain in interphase energy:

$$\Delta W_{\text{si}} \equiv \langle W(\text{semi})\rangle - \langle W(\text{incoh})\rangle \tag{33}$$

occurs during the transformation from the reference incoherent state to the semi-coherent state. This energy gain, however, is offset by additional intraphase strain energy contributions $\Delta\gamma^{\text{rel}}_{\text{intra}}$ that accompany this transformation. Thus, the relaxation of the incoherent reference state to achieve semi-coherency across the interface introduces a non-uniform lattice strain on both sides of the interface, which increases the elastic energy within each of the two phases. This non-uniform strain has the periodicity of the superlattice, or of the misfit dislocation network illustrated in figure 2(*d*). The significance of $\Delta\gamma^{\text{rel}}_{\text{intra}}$ may be illustrated by a harmonic oscillator model. If a harmonic oscillator is subjected to a force F that results in a displacement u, the consequent energy reduction $-Fu$ is offset by an energy increase $Fu/2$ stored in the harmonic spring, which yields a resultant energy gain of $-Fu/2$. By analogy, we assume that $\Delta\gamma^{\text{rel}}_{\text{intra}}$ reduces the energy gain from $\Delta\gamma^{\text{rel}}_{\text{inter}}$ by a factor of $1/2$. Thus

$$\Delta\gamma^{\text{rel}}_{\text{intra}} = \Delta W_{\text{si}}/2. \tag{34}$$

The development of better approximations to $\Delta\gamma_{\text{intra}}$ appears feasible, but will not be pursued here.

2.3.3. Relation to continuum treatments. With the results obtained in the last section, equation (24) can be rewritten as

$$\Delta\gamma = \Delta\gamma^{\text{strain}}_{\text{intra}} - \Delta W_{\text{si}}/2 + W_{h_1} - D \sum f_j W_{h_j}(\text{semi}) \tag{35}$$

where $\Delta\gamma^{\text{strain}}_{\text{intra}}$ is given in equations (18) and (20). We can now identify the terms in the lattice treatment that correspond to the strain and the dislocation contributions in the phenomenological relation, equation (14). We write the strain energy term in the form

$$\Delta\gamma(\text{strain}) = [E(A_{\text{bulk}}, 1, 0; 2) - E(A_{\text{coh}}, 1, \epsilon_m; 2)]/2S_{\text{bulk}} \tag{36}$$

which is analogous to the difference between the second term on the right-hand side of equation (14) evaluated with $\kappa = \epsilon_m/b_\perp$, and with $\kappa = 0$. The misfit dislocation energy is given by

$$\Delta\gamma(\text{disloc}) = \left[W_{h_1} - \sum f_j W_{h_j}(\text{semi})\right] + \Delta W_{\text{si}}/2 \tag{37}$$

where the term in brackets represents the interphase contribution and the final term is the intraphase contribution. Roughly speaking, the interphase contribution corresponds to the dislocation core energy and the intraphase contribution to the elastic strain-field energy. $\Delta\gamma$(disloc) is analogous to the first term on the right-hand side of equation (14). A formulation of the misfit dislocation line energy λ derived from continuum theory is given in [83]. The lattice formulation, although approximate, is more direct and explicit than the continuum formulation.

The sum of the strain energy and the dislocation energy contributions, equations (36) and (37), does not account for the entire interface energy change given in equation (35). The remaining terms, which correspond to the difference $\Delta\gamma - \Delta\gamma(\text{strain}) - \Delta\gamma(\text{disloc})$, will be referred to as stoichiometric contributions, since they are proportional to the change in stoichiometry, $d = D - 1$, that accompanies the transformation from the coherent to the semi-coherent interface:

$$\Delta\gamma(\text{stoich}) = d\left[E(A_{\text{coh}}, 1, \epsilon_m; 2)/2S_{\text{coh}} - \sum f_j W_{h_j}(\text{semi}) - \mu_2 N_2/2S_{\text{coh}}\right]. \tag{38}$$

The first two terms on the right-hand side of equation (38) give the intraphase and interphase contributions, respectively, to the interface energy associated with the fraction d of phase-2 atoms transferred from the thermodynamic reservoir to the interface cell. The final term represents the energy cost to remove the atoms from the reservoir.

The total change in interface energy that accompanies the transformation from the coherent to the semi-coherent state:

$$\Delta\gamma = \Delta\gamma(\text{strain}) + \Delta\gamma(\text{disloc}) + \Delta\gamma(\text{stoich}) \tag{39}$$

is thus expressed in a form more readily interpreted than equation (35). In doing this, we were led to the consideration of a stoichiometric contribution that does not arise in continuum treatments. In the numerical application presented below, however, the stoichiometric term is small, numerically. We note, however, that $\Delta\gamma$(stoich), like $\Delta\gamma$(strain), is volume dependent.

In absolute value, the strain term is generally a larger contribution to $\Delta\gamma$ than the dislocation term, except perhaps in the case of small perpendicular cell dimensions, $A_\perp$. We note that the dislocation term depends on the assumed form of the misfit dislocation network, and therefore is not necessarily unique. In favourable cases, calculation of $\Delta\gamma$(disloc) may enable a prediction of the most stable dislocation network configuration.

3. Numerical example: carbide–matrix interface

To demonstrate the formulation presented in the previous section, it is applied here to the interface between the (001) face of tetragonal TiAl and the (001) face of perovskite Ti_3AlC. The strengthening effect of carbide precipitates in a TiAl matrix [90, 91] is of interest for structural applications of titanium aluminide alloys at high temperatures. Although the carbide precipitates in real specimens occur in the form of inclusions, the numerical calculations performed here utilize the multilayer geometry employed in our previous exposition.

The selected interface differs from our idealized illustration, figure 2, in that the layer unit cells are face-centred square rather than primitive square. A simplifying feature of square lattices in general is that faulting does not occur.

First principles local density functional theory calculations are performed with the VASP code [92]. The calculations employed the Perdew–Wang 1991 version [93] of the generalized gradient approximation.

3.1. Bulk properties

Calculations of the equilibrium lattice constants using the conventional four-atom face-centred-tetragonal TiAl unit cell yielded $a_{\mathrm{TiAl}} = 3.96$ Å and $c_{\mathrm{TiAl}} = 4.08$ Å. For the perovskite carbide, we obtained $a_{\mathrm{Ti_3AlC}} = 4.18$ Å. For comparison, the experimentally observed lattice constants are $a(1) \equiv a_{\mathrm{TiAl}} = 4.005$ Å, $c(1) \equiv a_{\mathrm{TiAl}} = 4.07$ Å, and $a(2) \equiv a_{\mathrm{Ti_3AlC}} = 4.15$ Å. Substituting the observed lattice constants in equation (1) gives a misfit $\epsilon_m = 0.035$, which is slightly smaller than the theoretically predicted value.

We mentioned previously that chemical potentials for one or more components are not always uniquely determined for multicomponent heterophase interface systems [59, 60, 72]. For a TiAl stoichiometry that is slightly Ti rich with respect to the equiatomic composition, however, a second phase, α_2-Ti_3Al, is present, in equilibrium with γ-TiAl over a range of temperature [94]. In the presence of three phases (the two aluminides and the perovskite carbide), all of the chemical potentials are fixed (at a particular temperature and pressure). Their values may be determined by solving simultaneously the equations

$$\mu_{\mathrm{Ti}} + \mu_{\mathrm{Al}} = \mu_{\mathrm{TiAl}} \tag{40}$$

and

$$3\mu_{\mathrm{Ti}} + \mu_{\mathrm{Al}} = \mu_{\mathrm{Ti_3Al}}. \tag{41}$$

We ignore in this analysis the constitutional defects that are present in the real materials, as well as the resultant deviations from ideal stoichiometry. By this procedure, we obtain $\mu_{\mathrm{Ti}} = -7.89$ eV, and $\mu_{\mathrm{Al}} = -4.37$ eV. With these results, the carbon chemical potential

$$\mu_{\mathrm{C}} = \mu_{\mathrm{Ti_3AlC}} - 3\mu_{\mathrm{Ti}} - \mu_{\mathrm{Al}} = -11.04 \text{ eV}. \tag{42}$$

3.2. Coherent interface

To treat the coherent interface, we consider a unit cell in the plane of the interface with basis vectors $(A_{1x}, A_{1y}) = (1, 0)a(1)$ and $(A_{2x}, A_{2y}) = (0, 1)a(1)$. The corresponding interface area is $2S = 2a(1)^2$ per unit cell. The sequence of (001) face-centred-tetragonal TiAl layers alternates between pure layers of the two components, with layer atomic positions either at edge-centre $(\frac{1}{2}, 0)$ and $(0, \frac{1}{2})$ sites or at the origin (0, 0) and face-centred $(\frac{1}{2}, \frac{1}{2})$ sites. The perovskite Ti_3AlC (001) layers alternate between TiAl layers (with Ti at $(\frac{1}{2}, \frac{1}{2})$ and Al at (0, 0)) and Ti_2C layers (Ti at $(\frac{1}{2}, 0)$, $(0, \frac{1}{2})$ and C at $(\frac{1}{2}, \frac{1}{2})$).

Four interface terminations enter the consideration, which correspond to combinations of the terminations of each of the phases: TiAl termination/Ti_3AlC termination = Ti/Ti_2C, Al/Ti_2C, Al/TiAl and Ti/TiAl. Each of these interfaces has three inequivalent parallel translation states, $T_1 = (0, 0)$, $T_2 = (\frac{1}{2}, 0)$ and $T_3 = (\frac{1}{4}, \frac{1}{4})$. The (0, 0) translation state refers to layers with the following atomic configurations: Ti termination of TiAl: Ti atomic positions (0, 0), $(\frac{1}{2}, \frac{1}{2})$; Al termination of TiAl: Al atomic positions (0, 0), $(\frac{1}{2}, \frac{1}{2})$; TiAl termination of Ti_3AlC: Ti at $(\frac{1}{2}, \frac{1}{2})$, Al at (0, 0); Ti_2C termination of Ti_3AlC: Ti at $(\frac{1}{2}, 0)$, $(0, \frac{1}{2})$, C at $(\frac{1}{2}, \frac{1}{2})$.

The remaining translation states are obtained by a translation T_j of either of the phases with respect to the other. Altogether, there are $4 \times 3 = 12$ coherent (001) TiAl/Ti_3AlC interface configurations, in view of the four terminations and the three possible translation states for each.

Multilayer supercells (figure 1) were constructed with nine layers each of TiAl and Ti_3AlC. In the case of the TiAl(Ti)/$Ti_3AlC(Ti_2C)$ interface, for example (where the terminating layer of each phase is indicated in parentheses), there are five Ti and four Al layers in the TiAl slab, five Ti_2C and four TiAl layers in the Ti_3AlC slab, and a total of 41 atoms in the unit cell.

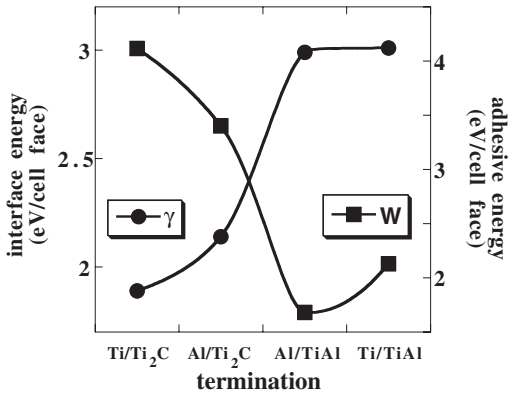

Figure 4. Calculated interface energies (filled circles, ordinate scale on the left-hand side of the figure) and adhesive energies (filled squares, ordinate scale on the right-hand side of the figure), in units of electron volts per unit-cell face area (a^2), for the four possible terminations of a coherent interface between tetragonal TiAl and perovskite Ti_3AlC. The interface orientation, for both phases, is (001). Results shown are for the low-energy translation state, T_1. The energetically preferred termination, with the lowest interface energy and highest adhesive energy, corresponds to a Ti layer of TiAl opposite a Ti_2C layer of Ti_3AlC. Curves drawn between points are to guide the eye.

The k-point set was selected by the Monkhorst–Pack procedure [95] with indices (8, 8, 2), which resulted in ten k-points.

In the coherent-interface calculations presented in this section, we employed cell dimensions $A_1 = A_2 = a(1) = 3.96$ Å. With A_1 and A_2 fixed, calculations were performed for a series of perpendicular cell dimensions A_3 to determine the optimal value. By employing the calculated total energy E of the multilayer cell, in conjunction with the chemical potentials determined by equations (40)–(42), the interface energy given in equation (6) can be evaluated. In the case of the TiAl(Ti)/$Ti_3AlC(Ti_2C)$ interface, for example, we have

$$2\gamma_{\rm coh}S_{\rm coh} = E_{\rm Ti/Ti_2C} - 24\mu_{\rm Ti} - 12\mu_{\rm Al} - 5\mu_{\rm C} \tag{43}$$

where $E_{\rm Ti/Ti_2C}$ is the energy of the supercell.

For comparison, the adhesive energy:

$$2W_{\rm coh}S_{\rm coh} = E_{\rm Ti/Ti_2C} - E_{\rm Ti}(1) - E_{\rm Ti_2C}(2) \tag{44}$$

was also calculated. Here $E_{\rm Ti}(1)$ and $E_{\rm Ti_2C}(2)$ refer to slabs of phase 1 and phase 2 with the appropriate terminations. The translation state T_1 was energetically preferred for all terminations. The energies γ and W for this translation state are plotted in figure 4 for the four terminations. Note that the interface energy (ordinate scale on the left-hand side) varies essentially inversely with the adhesive energy (ordinate scale on the right-hand side). The preferred interface configuration corresponds to the Ti termination of TiAl opposite the Ti_2C termination of Ti_3AlC. For this interface, the strong Ti–C bonds across the interface result in the lowest interface energy, $\gamma_{\rm coh}S_{\rm coh} = 1.9$ eV, and the highest adhesive energy, $W_{\rm coh}S_{\rm coh} = 4.2$ eV.

3.3. Corrections to the coherent-interface energy

Corrections to the coherent-interface energy are formulated in equations (36)–(39). Results are presented only for the low-energy termination Ti/Ti_2C. The largest correction is the (uniform)

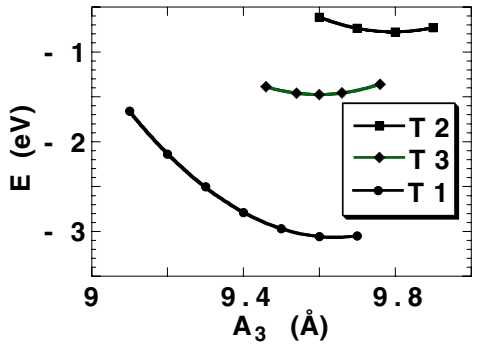

Figure 5. Energy per interface unit cell for the low-energy termination (Ti/Ti_2C) of the TiAl/Ti_3AlC interface as a function of cell dimension A_3 perpendicular to the interface. Results are shown for three parallel translation states T_j. The ordinate scale is shifted by 290 eV. The translation state T_1 is energetically preferred for all of the terminations considered in figure 1. Calculations of the coherent-interface energy, based on equation (1), employ the results for translation state T_1. The other translation states are used in calculations of $\Delta\gamma$(disloc).

strain term, $\Delta\gamma_{\text{strain}}$. To normalize the results to the unit-cell area of the coherent cell, we rewrite equation (36) as

$$2\,\Delta\gamma(\text{strain})S_{\text{coh}} = D[E(A_{\text{bulk}}, 1, 0; 2) - E(A_{\text{coh}}, 1, \epsilon_m; 2)] \tag{45}$$

using the relation $S_{\text{coh}} = DS_{\text{bulk}}$. Calculations for a slab of phase 2 yielded an equilibrium lattice constant of $a(2) = 4.16$ Å. The corresponding (theoretical) misfit $\epsilon_m = (3.96 - 4.16)/4.16 = -0.048$. In the following, we employ the theoretical value rather than the observed misfit, $\epsilon_m = -0.035$. With $\epsilon_m = -0.048$, we obtain $d = -0.093$ and $D = 0.91$. The correction to γ associated with strain is then

$$\Delta\gamma(\text{strain})S_{\text{coh}} = 0.96 \text{ eV}. \tag{46}$$

Next we consider the dislocation term, $\Delta\gamma$(disloc). In figure 5 the cell energy for the (energetically preferred) Ti/Ti_2C termination as a function of perpendicular cell coordinate A_3 for the three parallel translation states, T_j, is plotted. The energy zero on the ordinate scale is shifted by 290 eV. Using these results as well as energies for the corresponding isolated slabs, adhesive energy differences $2\,\Delta W_{h_2}(\text{semi}) = -2.3$ eV and $2\,\Delta W_{h_3}(\text{semi}) = -1.4$ eV for the relaxed coherent interfaces and $2\,\Delta W_{h_2}(\text{incoh}) = -6.8$ eV and $2\,\Delta W_{h_3}(\text{incoh}) = -3.0$ eV for the reference incoherent interfaces are obtained. With these energies, in conjunction with the fractions $f_j(\text{semi})$, we calculate the intraphase contribution to $\Delta\gamma$(disloc).

The weights $f_j(\text{semi})$ depend on the structure of the misfit dislocation network. According to figure 5, translation state T_2 is the most unfavourable one, and points with this symmetry are assumed to represent intersection points of the misfit dislocation network in the semi-coherent interface. Accordingly, the misfit dislocation lines are assumed to run in the [110] directions parallel to the interface. These misfit dislocation lines, which are of edge character, are depicted schematically by the solid lines in figure 6. The top panel of this figure illustrates four interface unit cells, where the dashed lines indicate cell boundaries. These unit cells correspond to periodicity $\epsilon_m^{-1} = n = 21$. In the directions (0, 1) and (1, 0), there are 20 primitive-cell units of phase 2 for every 21 units of phase 1. The square unit cell with dimensions $A_{\text{super}} = 20a(2)$ therefore contains $20 \times 20 = 400$ Ti_2C primitive-cell units. Regions of the cell distant from the dislocation lines, near the point labelled T, and symmetrically equivalent points, may be regarded as essentially coherent patches. These patches correspond to the strongest

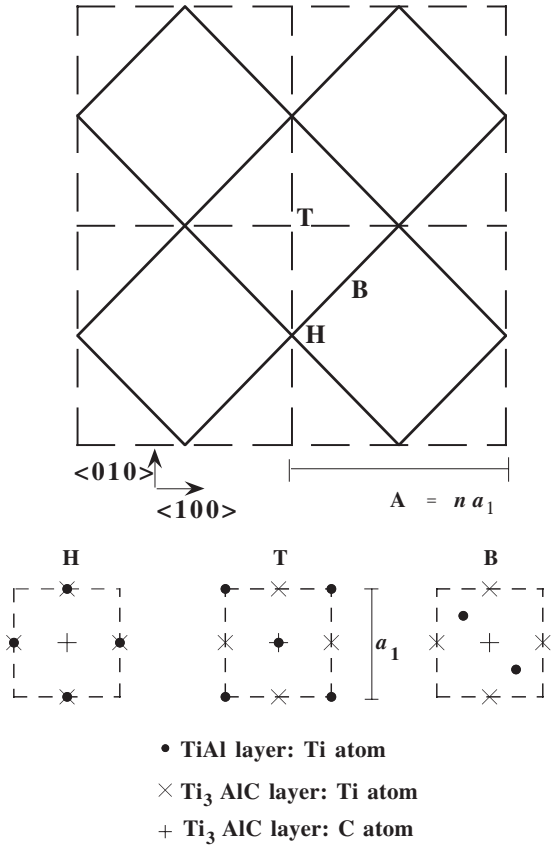

Figure 6. A schematic diagram of the periodic unit cell of the (Ti/Ti_2C)-terminated TiAl/Ti_3AlC interface. Broken lines in the top panel denote boundaries of square cells with dimension $A \approx 20a_1$. Solid lines denote misfit dislocations. Symmetry points T, H and B denote sites of on-top, hollow and bridge-type symmetry. Local atomic configurations in the vicinity of these sites are depicted in the lower three panels, for which the linear scale is multiplied by about 10, relative to that of the upper panel. In the regions of best interfacial bonding, in the vicinity of points equivalent to T, Ti atoms in TiAl lie directly above C atoms in the carbide.

interface bonding, with TiAl Ti atoms (filled circles) located on top of perovskite carbon atoms (plus symbols); the B and H configurations, which correspond to translation states T_3 and T_2 in figure 5, are less well bonded. The lower panels of figure 6 show approximate atomic configurations in the vicinity of the on-top, bridge and hollow (T, B and H) sites, respectively. The scale of these lower panels is magnified by about a factor of 10 relative to that of the upper panel.

From these considerations, we estimate that two primitive-cell units are located at misfit dislocation line intersections (T_2- or H-like sites) and $2 \times 20 - 2 = 38$ (carbide) primitive-cell units are located along the misfit dislocation lines (T_3- or B-like sites) of the semi-coherent interface. The remaining 360 atoms lie in T-like sites. Accordingly, $f_3(\text{semi}) = 38/400 = 0.095$ and $f_2(\text{semi}) = 2/400 = 0.005$. With these results, the interphase contribution to the dislocation energy is

$$\Delta\gamma_{\text{inter}}(\text{disloc}) = f_2\,\Delta W_{h_2}(\text{semi}) + f_3\,\Delta W_{h_3}(\text{semi}) = 0.08\ \text{eV}. \tag{47}$$

The remaining contribution to the dislocation energy is $\Delta\gamma_{\text{intra}}(\text{disloc})$. Evaluation of this term requires values for $f_j(\text{incoh})$. Taking these values to be proportional to the relative number of sites in the unit cell of a given symmetry, we have $f_1(\text{incoh}) = 0.25$, $f_2(\text{incoh}) = 0.25$ and $f_3(\text{incoh}) = 0.50$. Then, expressing ΔW_{si} in the form

$$\Delta W_{\text{si}} = D \sum \left[f_j(\text{semi})\, \Delta W_{h_j}(\text{semi}) - f_j(\text{incoh})\, \Delta W_{h_j}(\text{incoh}) \right] \tag{48}$$

we obtain

$$\Delta W_{\text{si}} = 1.35 \text{ eV} \tag{49}$$

and equation (35) then gives

$$\Delta\gamma_{\text{intra}}^{\text{rel}} = 0.68 \text{ eV}. \tag{50}$$

We consider now the stoichiometric contribution to the interface energy correction, given in equation (38). Although the individual contributions are large, their sum is essentially zero, to within hundredths of an electron volt. Substituting the numerical results for the terms on the right-hand side of equation (39), we obtain

$$\Delta\gamma S_{\text{coh}} = -0.20 \text{ eV}. \tag{51}$$

Comparing this value with the result for a coherent interface, $\gamma_{\text{coh}} S_{\text{coh}} = 1.9$ eV, we find that the correction to the coherent-interface result is relatively small, of the order of 10%. For the chosen cell size, a great deal of cancellation occurs between the strain term $\Delta\gamma(\text{strain})$ and the intraphase relaxation term, $\Delta\gamma_{\text{intra}}^{\text{rel}}$. (Recall that the strain term is volume dependent, as indicated by equation (8), and γ_{coh} therefore varies with the perpendicular cell dimension.)

We do not present here an assessment of the physical significance of the calculated interface energies for the TiAl/Ti_3AlC interface. Before such an assessment is attempted, the accuracy of the formulation should first be demonstrated. Possible approaches to test this accuracy are discussed in the following subsection.

3.4. Accuracy of correction terms

The practical usefulness of the approach presented in section 2.3 of this paper depends on the accuracy of the formulation of the terms on the right-hand side of equation (39). The additivity assumption invoked at the outset, equation (16), is difficult to avoid, but other aspects of the treatment can perhaps be refined. For example, the bonding across the interface was assumed linear:

$$D \equiv f(d) = 1 + d. \tag{52}$$

To improve accuracy, it may be possible to correct $f(d)$, and perhaps other terms, approximately, for many-body effects.

A critical approximation is made in the treatment of the intraphase part of the relaxation energy, $\Delta\gamma_{\text{intra}}^{\text{rel}}$, equation (34), which was found to be a large term numerically. One possible approach for testing equation (34) would be to perform a simulation for a heterophase interface for which interatomic potentials are available. For such an interface, the energy for the semi-coherent interface could be evaluated by direct simulation, and then compared to approximate calculations. An alternative approach would be to perform first-principles calculations for distorted slabs of phases 1 and 2 separately. In each, the top layers would be frozen in a distorted configuration intended to mimic the interface layers of the semi-coherent interface. The increase in energy, compared with undistorted slabs, would give a more direct estimate of $\Delta\gamma_{\text{intra}}^{\text{rel}}$ than equation (34).

Another approach for checking the accuracy of the formulation would be to verify the consistency of results obtained with cells of different sizes. Thus one could perform first-principles calculations of γ_{semi}, based on the approach of section 2.3, for cells with different dimensions either parallel or perpendicular to the interface. It would be useful, for example, to verify that the results are independent of $A_\perp$. With regard to the parallel dimension, $A_\parallel$, calculations for values of $n > 1$ that are numerically feasible, even though smaller than those dictated by the inverse of ϵ_m, would be helpful for testing.

Yet another way to test the consistency of the formulation is to vary the dimensions of the coherent interface. In our discussion, we have assumed that phase 2 is strained to achieve coherency with (unstrained) phase 1. If the identities of phase 1 and phase 2 are switched, the result for the interface energy of (unstrained) semi-coherent interface should be unchanged, in principle.

The tests of accuracy and consistency outlined in this section remain to be performed. Clearly, such tests should be conducted to determine the reliability of the method.

4. Discussion

In this paper, three approaches for calculating interface energies for heterophase interfaces have been discussed. The first technique employs first-principles methods to treat a large supercell whose dimensions correspond to the misfit dislocation spacing, n. The second technique involves a similar approach, but utilizes classical interatomic potentials instead of first-principles calculations. The third technique, to which the most attention has been devoted, involves first-principles calculations on much smaller cell sizes, and invokes approximations to estimate contributions of different types to the total energy. A numerical demonstration of the third technique for a carbide interface with titanium aluminide was presented.

For computational reasons, the first technique is severely limited in the interface systems to which it is applicable. The second technique is also currently restricted by the dearth of suitable potentials for heterophase interfaces. Nevertheless, environmentally sensitive potentials have been developed to a great extent over the past two decades, and there appears to be considerable scope for continued improvement. It may eventually be possible to develop potentials for multicomponent systems that interpolate accurately between a range of coordination environments such that a single unified classical potential can describe both the interface region and the two respective bulk phases of a system of interest. Perhaps only the second technique has promise for treating high temperatures and mechanical properties. The third technique, described in some detail, has the advantage that it is currently tractable and suitable for application to virtually any interface between inorganic crystalline phases. The accuracy of this technique, however, needs thorough investigation. If this approach can be proven effective for pristine interfaces, its extension for treating interface impurities can be considered.

In our opinion, all three techniques are important for the future development of interface computation. The first technique, although restricted, can provide benchmark results that can serve as tests for the other two methods. The second and third techniques can also provide useful tests for each other.

Acknowledgments

RB and DNS were supported at Northwestern University by US Department of Energy grant DEFG02-96ER45597. CW was supported by the Air Force Office of Scientific Research at the US Air Force Research Laboratory, Materials and Manufacturing Directorate, Wright

Patterson AFB, under contract No F33615-96-C-5258. This work was supported in part by a grant of computer time from the DoD High Performance Computing Modernization Program, at the Aeronautical Systems Center—Major Shared Resource Center, on the IBM-SP3. This project also received a grant of computer time at the National Energy Research Computer Center at Lawrence Berkeley Laboratory.

References

[1] Groen H B, Kooi B J, Vellinga W P and De Hosson J Th M 1999 *Phil. Mag.* A **79** 2083
[2] Ikuhara Y and Pirouz P 1998 *Microsc. Res. Tech.* **40** 206
[3] Rühle M 1997 *J. Surf. Anal. (Japan)* **3** 157
[4] Muller D A, Shashkov D A, Benedek R, Yang L H, Silcox J and Seidman D N 1998 *Phys. Rev. Lett.* **80** 4741
[5] Xin Y, James E M, Browning N D and Pennycook S J 2000 *J. Electron Microsc.* **49** 231
[6] Shashkov D A, Chisholm M F and Seidman D N 1999 *Acta Mater.* **47** 3939
[7] Chan D K, Seidman D N and Merkle K L 1995 *Phys. Rev. Lett.* **75** 1118
[8] Shashkov D A, Muller D A and Seidman D N 1999 *Acta Mater.* **47** 3953
[9] Voigtlander B and Theuerkauf N 2000 *Surf. Sci.* **461** L575
[10] de la Figuera J, Schmid A K, Bartelt N C, Pohl K and Hwang R Q 2001 *Phys. Rev.* B **63** 165431
[11] Renaud G S 2001 *Surf. Rev. Lett.* **7** 437
[12] Christensen A and Carter E A 2001 *J. Chem. Phys.* **114** 5816
[13] Raic K T 2000 *Ceram. Int.* **26** 19
[14] Lin C C, Chen R B and Shiue R K 2001 *J. Mater. Sci.* **36** 2145
[15] Garofalini S H 2000 *J. Power Sources* **89** 190
[16] Chen J, Gu M and Pan F 2001 *Metall. Mater. Trans.* A **32** 2033
[17] Ma J and Tan G E B 2001 *J. Mater. Process. Technol.* **113** 446
[18] Leo P H and Johnson W C 2001 *Acta Mater.* **49** 1771
[19] Umantsev A 2001 *Phys. Rev.* B **64** 5419
[20] Halley J W, Schelling P and Duan Y 2000 *Electrochim. Acta* **46** 239
[21] Cline T W and Withers P J 1995 *An Introduction to Metal Matrix Composites* (New York: Cambridge University Press)
[22] See, for example, Eshelby J D 1976 *Progress in Solid Mechanics* ed I Sneddon and R Hill (Amsterdam: North-Holland) p 89
[23] Payne M C, Teter M P, Allan D C, Arias T A and Joannopoulos J 1992 *Rev. Mod. Phys.* **64** 1045
[24] Harrison W A 1989 *Electronic Structure and the Properties of Solids* (Mineola, NY: Dover)
[25] Levay A, Möbus G, Vitek V, Rühle M and Tichy G 1999 *Acta Mater.* **47** 4143
[26] Ernst F 1993 *Phil. Mag.* A **68** 1251
[27] Switzer J A, Shumsky M G and Bohannan E W 1999 *Science* **284** 293
[28] De Hosson J T M, Goren H B, Kooi B J and Vitek V 1999 *Acta Mater.* **47** 4077–92
[29] Frank F C and van der Merwe J H 1949 *Proc. R. Soc.* A **198** 205
[30] van der Merwe J H 1950 *Proc. Phys. Soc.* A **63** 616
[31] Matthews J and Blakeslee A E 1974 *J. Cryst. Growth* **27** 118
[32] Bonnet R 1981 *Phil. Mag.* A **43** 1165
[33] Bonnet R, Labradou M and Penisson J M 1992 *Phys. Rev. Lett.* **69** 104
[34] Bonnet R 1996 *Phil. Mag.* A **73** 1193
[35] Bonnet R, Youssef S B and Fnaiech M 2001 *Mater. Sci. Eng.* A **297** 286 and references therein
[36] Gumbsch P, Daw M S, Foiles S M and Fischmeister H F 1991 *Phys. Rev.* B **43** 13 833
[37] Wolf D and Yip S (ed) 1992 *Materials Interfaces: Atomic-Level Structure and Properties* (New York: Chapman and Hall)
[38] Daw M and Baskes M I 1984 *Phys. Rev.* B **29** 6443
Foiles S M, Baskes M I and Daw M S 1986 *Phys. Rev.* B **33** 7983
[39] Gilmore C M 1989 *Phys. Rev.* B **40** 6402
[40] Dregia S A, Wynblatt P and Bauer C L 1987 *J. Vac. Sci. Technol.* A **5** 1746
[41] Gumbsch P 1991 *PhD Dissertation* University of Stuttgart
[42] Asta M, Foiles S M and Quong A A 1998 *Phys. Rev.* B **57** 11 265
[43] Angelo J E and Baskes M I 1996 *Interface Sci.* **4** 47
[44] Baskes M I 1992 *Phys. Rev.* B **46** 2727
[45] Christensen A, Ruban A V, Stoltze P, Jacobsen K W, Skriver H L, Norskov J K and Besenbacher F 1997 *Phys. Rev.* B **56** 5822

[46] Jacobsen J, Nielsen L P, Besenbacher F, Stensgaard I, Laegsgaard E, Rasmussen T, Jacobsen K W and Norskov J K 1995 *Phys. Rev. Lett.* **75** 489
[47] Rasmussen T 2000 *Phys. Rev.* B **62** 12 664
[48] Deutsch T, Bayle P, Lancon F and Thibault J 1995 *J. Phys.: Condens. Matter* **7** 6407
[49] Sayle D C and Watson G W 2000 *Phys. Chem. Chem. Phys.* **2** 5491
Sayle D C and Watson G W 2001 *Surf. Sci.* **473** 97
[50] Ohira T, Inoue Y, Murata K and Murayama J 2001 *Appl. Surf. Sci.* **171** 175
[51] Zepeda-Ruiz L A, Maroudas D and Weinberg W H 1999 *J. Appl. Phys.* **85** 3677
[52] Ebbsjo I, Kalia R K, Nakano A, Rino J P and Vashishta P 2000 *J. Appl. Phys.* **87** 7708
[53] Albe K, Nordlund K, Nord J and Kuronen A 2001 submitted
[54] Oyama N, Ohta E, Takeda K, Shiraishi K and Yamaguchi H 1999 *Surf. Sci* **433–5** 900
[55] Duffy D M, Harding J H and Stoneham A M 1992 *Acta Metall. Mater.* **40** S11
Duffy D M, Harding J H and Stoneham A M 1993 *Phil. Mag.* A **67** 865
[56] Purton J, Parker S C and Bullett D W 1997 *J. Phys.: Condens. Matter* **9** 5709
Purton J A, Bird D M, Parker S C and Bullett D W 1999 *J. Chem. Phys.* **110** 8090
[57] Schönberger U, Andersen O K and Methfessel M 1992 *Acta Metall. Mater. (Suppl.)* **40** S1
[58] Li C, Wu R, Freeman A J and Fu C L 1993 *Phys. Rev.* B **48** 8317
[59] Batirev I G, Alavi A, Finnis M W and Deutsch T 1999 *Phys. Rev. Lett.* **82** 1510
[60] Zhang W and Smith J R 2000 *Phys. Rev. Lett.* **85** 3225
[61] Schweinfest R, Köstlmeier S, Ernst F, Elsässer C and Wagner T 2001 *Phil. Mag.* A **81** 927
[62] Jarvis E A A, Christensen A and Carter E A 2001 *Surf. Sci.* **487** 55
[63] Batyrev I G and Kleinman L 2001 *Phys. Rev.* **64** 3410
[64] Adams J B, Hector L G, Siegel D J, Yu H and Zhong J 2001 *Surf. Interface Anal.* **31** 619
[65] Guo C X, Ellis D E, Dravid V P and Brewer L 2001 *Mater. Res. Soc. Symp. Proc.* vol 654, ed C B Carter *et al* AA5
[66] Hoekstra J and Kohyama M 1998 *Phys. Rev.* B **57** 2334
[67] Stadler R, Vogtenhuber D and Podloucky R 1999 *Phys. Rev.* **60** 17 112
[68] Dudiy S V, Hartford J and Lundqvist B I 2000 *Phys. Rev. Lett.* **85** 1898
[69] Dudiy S V and Lundqvist B I 2000 *Phys. Rev.* B **64** 5403
[70] Kelsey A and Ackland G J 1999 *Modell. Simul. Mater. Sci. Eng.* **7** 311
[71] Stirling A, Pasquarello A, Charlier J C and Car R 2000 *Phys. Rev. Lett.* **85** 2773
[72] Lambrecht W R L and Segall B 1992 *Acta Metall. Mater.* **40** S17
[73] Goniakowski J and Noguera C 1999 *Phys. Rev.* B **60** 16 120
[74] Benedek R, Alavi A, Seidman D N, Yang L H, Muller D A and Woodward C 2000 *Phys. Rev. Lett.* **84** 3362
[75] Albe K, Benedek R, Seidman D N and Averback R S *Mater. Res. Soc. Symp. Proc.* vol 654, ed C B Carter *et al* AA4.3
[76] Streitz F H and Mintmire J W 1994 *Phys. Rev.* B **50** 11 996
[77] Brenner D W 2000 *Phys. Status Solidi* b **217** 23
[78] Qian G X, Martin R M and Chadi D J 1989 *Phys. Rev.* B **38** 7649
[79] Backhaus-Ricoult M 2000 *Acta Mater.* **48** 4365
[80] Heine V 1980 *Solid State Physics* vol 35, ed D Turnbull and H Ehrenreich (New York: Academic)
[81] Benedek R 1978 *J. Phys. F: Met. Phys.* **8** 1119
[82] Timoshenko S P and Goodier J N 1970 *Theory of Elasticity* (New York: McGraw-Hill) p 39
[83] De Hosson J Th M and Kooi B 2001 *Surf. Interface Anal.* **31** 637
[84] Sutton A P and Balluffi R W 1995 *Interfaces in Crystalline Materials* (Oxford: Clarendon)
[85] Mader W and Knauss D 1992 *Acta Metall. Mater.* **40** S207
[86] Dehm G, Rühle M, Ding G and Raj R 1995 *Phil. Mag.* B **71** 1111
[87] Bollmann W 1972 *Surf. Sci.* **31** 1
[88] Finnis M W 1996 *J. Phys.: Condens. Matter* **8** 5811
[89] Tersoff J and Tromp R M 1993 *Phys. Rev. Lett.* **70** 2782
[90] Chen S, Beaven P A and Wagner R 1992 *Scr. Metall.* **26** 1205
[91] Gouma P I, Mills M J and Kim Y W 1998 *Phil. Mag. Lett.* **78** 59
[92] Kresse G and Furthmüller J 1996 *Comput. Mater. Sci.* **6** 15
Kresse G and Furthmüller J 1996 *Phys. Rev.* B **54** 11 169
[93] Perdew J P and Wang Y 1992 *Phys. Rev.* B **45** 13 244
[94] Ohnuma I, Fujita Y, Mitsui H, Ishikawa K, Kainuma R and Ishida K 2000 *Acta Mater.* **48** 3113
[95] Monkhorst H J and Pack J D 1976 *Phys. Rev.* B **13** 5188